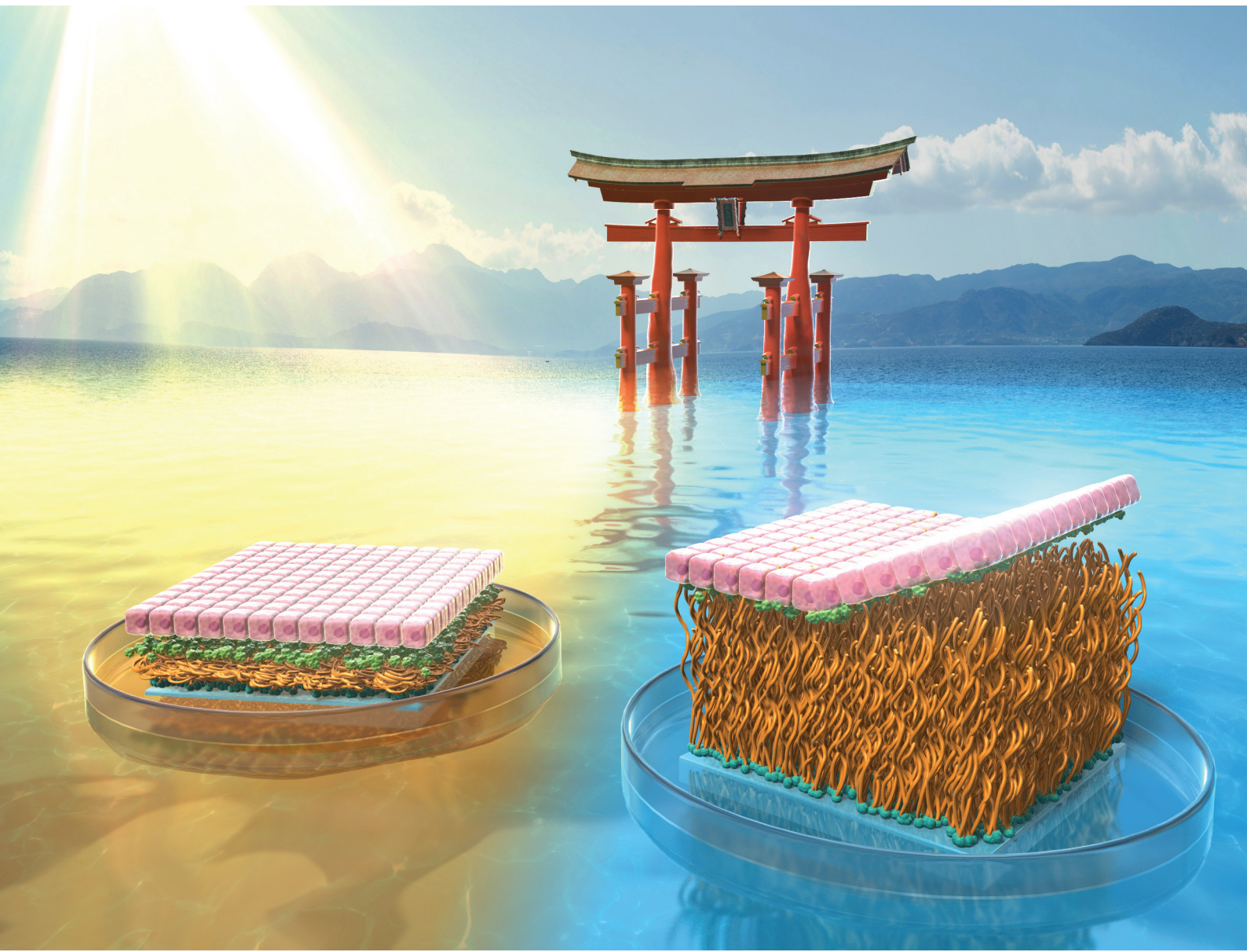


# Biomaterials Science

[rsc.li/biomaterials-science](https://rsc.li/biomaterials-science)



ISSN 2047-4849

## PAPER

Kenichi Nagase *et al.*  
Effective cell sheet preparation using  
thermoreversible polymer brushes with various  
graft densities and chain lengths



Cite this: *Biomater. Sci.*, 2025, **13**, 1657

## Effective cell sheet preparation using thermoresponsive polymer brushes with various graft densities and chain lengths<sup>†</sup>

Kenichi Nagase, <sup>\*a,b</sup> Minami Watanabe, <sup>b,c</sup> Akihiko Kikuchi <sup>c</sup> and Teruo Okano <sup>b,d</sup>

Various cell sheets have been used as effective and useful cellular tissues in tissue engineering and regenerative therapy. Poly(*N*-isopropylacrylamide) (PNIPAAm)-modified surfaces have been investigated for effective cell sheet preparation. In this study, the effective PNIPAAm graft density and chain length of PNIPAAm brushes for various cell types were investigated. The PNIPAAm brush-grafted glass was prepared via silanization and subsequent atom transfer radical polymerization (ATRP). The density of the PNIPAAm brushes was modulated by changing the ATRP initiator and co-adsorber composition, while the PNIPAAm brush length was modulated by changing the monomer concentration in the ATRP. The hydrophilicity of the PNIPAAm brushes increased with increasing PNIPAAm brush length because long PNIPAAm brushes tended to hydrate. Fibronectin adsorption increased with decreasing PNIPAAm brush concentration because the exposed hydrophobic co-adsorber in the dilute PNIPAAm brush enhanced the adsorption of fibronectin. The cell-sheet fabrication ability was investigated using six types of PNIPAAm brushes. An endothelial cell sheet was fabricated using a dense, short PNIPAAm brush. NIH/3T3 sheets can be fabricated using three types of PNIPAAm brushes: dense-long PNIPAAm brushes, moderately dense-short PNIPAAm brushes, and dilute-long PNIPAAm brushes. MDCK cell sheets could not be prepared using the PNIPAAm brushes. A549 cell sheets were prepared using a dense-short PNIPAAm brush and moderately dense-short PNIPAAm brushes. These results indicate that the optimal PNIPAAm brush conditions for cell sheet preparation vary depending on cell type. Thus, modulation of PNIPAAm brush density and length is an effective approach for preparing target cell sheets.

Received 21st December 2024,  
Accepted 10th February 2025

DOI: 10.1039/d4bm01705f  
[rsc.li/biomaterials-science](http://rsc.li/biomaterials-science)

## 1. Introduction

In recent decades, tissue engineering and regenerative medicine have been investigated as effective therapies for intractable disease.<sup>1–5</sup> In particular, cell sheets have been investigated as functional cellular tissues and regenerative medicines. Cell sheets, which are monolayer cellular tissue, have an

extracellular matrix (ECM) basal surface and can be easily transplanted into host tissue because the ECM acts as a cell adhesive glue.<sup>6–10</sup> Thus, transplantation of cell sheets has been used as an effective cell transplantation therapy.<sup>3–5,11–14</sup> Additionally, dense cellular tissue can be fabricated by stacking cell sheets,<sup>15</sup> and has been investigated for various tissue engineering applications.<sup>16–18</sup>

Cell sheets are prepared using a thermoresponsive polymer, poly(*N*-isopropylacrylamide) (PNIPAAm)-modified culture dish.<sup>6</sup> PNIPAAm is a thermoresponsive polymer whose hydrophobicity changes with external temperature, which is attributed to hydration and dehydration.<sup>19,20</sup> Using the PNIPAAm property, various types of biomedical applications have been investigated, including drug delivery systems,<sup>21–26</sup> biosensors,<sup>27–30</sup> bioanalysis and diagnostic devices,<sup>31–38</sup> bioseparation systems,<sup>39–47</sup> and tissue culture substrates.<sup>6,48–55</sup> In the application of the thermoresponsive cell culture substrate, PNIPAAm is modified on the cell culture substrate. Cells are seeded to the PNIPAAm-modified culture dish at 37 °C. At this temperature, PNIPAAm becomes dehydrated and hydrophobic,

<sup>a</sup>Graduate School of Biomedical and Health Sciences, Hiroshima University, 1-2-3 Kasumi, Minami-ku, Hiroshima City, Hiroshima, 734-8553, Japan.

E-mail: [nagase@hiroshima-u.ac.jp](mailto:nagase@hiroshima-u.ac.jp); Fax: +81-82-257-5323; Tel: +81-82-257-5323

<sup>b</sup>Institute of Advanced Biomedical Engineering and Science, Tokyo Women's Medical University, 8-1 Kawada-cho, Shinjuku, Tokyo, 162-8666, Japan

<sup>c</sup>Department of Materials Science and Technology, Graduate School of Advanced Engineering, Tokyo University of Science, 6-3-1 Niijuku, Katsushika, Tokyo 125-8585, Japan

<sup>d</sup>Cell Sheet Tissue Engineering Center, Department of Pharmaceutics and Pharmaceutical Chemistry, Health Sciences, University of Utah, Salt Lake City, UT84112 Utah, USA

<sup>†</sup> Electronic supplementary information (ESI) available: Supplementary data and methods. See DOI: <https://doi.org/10.1039/d4bm01705f>

leading to cell adhesion to the PNIPAAm-modified dish. The adhered cells proliferate after incubation for 4–5 days, and the cells reach confluence. When the temperature is reduced to 20 °C, the PNIPAAm becomes hydrated and hydrophilic. The adhered monolayer cells (cell sheet) detach from the PNIPAAm dish because the adhered monolayer cells cannot adhere to hydrophilic PNIPAAm.

PNIPAAm-modified cell culture dishes have been investigated using various types of polymer modification methods.<sup>49,56–58</sup> Widely used PNIPAAm-modified dishes are prepared with electron-beam (EB) irradiation,<sup>6,59</sup> where in a thin layer of PNIPAAm hydrogel is modified on the culture dish. The PNIPAAm modification method is suitable for large-scale production. However, precise control of the thickness of the PNIPAAm layer is difficult. To control the thickness of the grafted PNIPAAm layer on the dish, living radical polymerizations such as atom transfer radical polymerization (ATRP) and reversible addition–fragmentation chain transfer (RAFT) polymerization have been introduced.<sup>60–64</sup> These living radical polymerizations can precisely control the polymer length, leading to the modulation of the PNIPAAm layer thickness and PNIPAAm amount on the dish. In particular, ATRP is suitable for modulating PNIPAAm brush density and chain length. The initiator density on the graft substrate can be modulated by changing the composition of the initiator-modified silane coupling reagent and co-adsorber silane coupling reagent in the silane coupling reaction.<sup>65</sup> Additionally, brush length can be modulated by changing the monomer concentration.<sup>66</sup> Thus, PNIPAAm brushes prepared with ATRP are an effective substrate because brush density and chain lengths can be modulated.

Cell adhesion and detachment on PNIPAAm-modified interfaces are significantly influenced by the adsorption of extracellular matrix (ECM), such as fibronectin on PNIPAAm-modified interfaces, because the ECM mediates cell adhesion.<sup>9,67</sup> During cell adhesion on the PNIPAAm-modified interface, ECM adheres on the interfaces, and cells adhere on the substrate using the pre-adsorbed ECM. In addition, cell detachment from the PNIPAAm-modified interface is induced by desorption of ECM from PNIPAAm-modified interfaces. Thus, ECM adsorption on PNIPAAm-modified interfaces significantly influences cells adhesion and detachment. A previous report indicated that PNIPAAm brush density influences the protein adsorption, because the dilute PNIPAAm brush exposes the graft interface, such as the hydrophobic silane layer, leading to enhanced adsorption of ECM.<sup>61</sup> Moreover, the PNIPAAm brush length effects ECM adsorption.<sup>60</sup> Long PNIPAAm brushes also exhibit lower fibronectin adsorption compared with that of short PNIPAAm brushes, which is attributed to the relatively hydrophilic property of long PNIPAAm brushes. Therefore, PNIPAAm brush density and chain length influence ECM adsorption/desorption, cell adhesion/detachment, and cell sheet fabrication/detachment properties.

Various cell sheets have been investigated for various applications. Endothelial cell sheets are used to enhance vascularization.<sup>68</sup> Fibroblast cell sheets are used for the treatment of

lung air leaks.<sup>14,69</sup> MDCK cell sheets have been investigated as kidney cell sheets and could be applied to kidney tissue engineering.<sup>10,70</sup> Cancer cell sheets can be used as *in vivo* or *in vitro* cancer tissue models.<sup>71–74</sup> These cells have different adhesive and detachment properties. Furthermore, previous research has investigated the relationship between PNIPAAm brush length and cell adhesion using various cell types.<sup>75</sup> The results show that PNIPAAm brush length influences cell adhesion, and that the optimal PNIPAAm brush length differs among cell types. Thus, the most suitable PNIPAAm structure also differs among cell types.

In this study, we investigated suitable PNIPAAm brush configurations, such as brush density and length, for each type of cell sheet preparation. PNIPAAm brushes of various densities and lengths were prepared using ATRP. Various cell sheets were prepared using the prepared PNIPAAm brushes.

## 2. Materials and methods

### 2.1. Preparation of thermo responsive polymer brushes with various chain length and densities

Thermoresponsive polymer brushes with various chain lengths and densities were prepared *via* a silane coupling reaction and subsequent ATRP (Fig. 1). All reagents are described in the ESI.† Cover glasses (24 × 50 mm) were placed in a glass holder. Glass surfaces were cleaned using a plasma cleaner (PX-1000; Samco, Kyoto, Japan). Cleaned cover glass containing a glass holder was placed in a 500 mL separable flask. Humidified nitrogen was poured into the flask, and the glass in the flask was incubated at 60% relative humidity and 25 °C for 1 h. Then, two types of silane coupling reagents, (chloromethyl) phenylethyl-trimethoxysilane (CPTMS) and phenethyl-trimethoxysilane (PETMS), were dissolved in the toluene in a molar ratio (CPTMS : PETMS) of 100 : 0, 50 : 50, or 25 : 75 in order to modulate ATRP initiator density. Typically, in the case of the 50 : 50 ratio, CPTMS (1.59 mL) and PETMS (1.81 mL) were dissolved in 292 mL of toluene. The prepared reaction solution was poured into a flask that had a cover glass. The silanization reaction was conducted at 25 °C for 18 h. After the reaction, cover glasses were rinsed with toluene and acetone, and then dried in a drying oven at 110 °C for 4 h. The prepared cover glasses with various initiator densities were named I100, I50, and I25 based on the CPTMS molar ratio in the silanization reaction.

PNIPAAm brushes were prepared *via* ATRP using initiator-modified glasses of various densities. Two types of *N*-isopropylacrylamide (NIPAAm) solutions were prepared to modulate the PNIPAAm brush length by changing the monomer concentration during ATRP: NIPAAm (12.7 g, 113 mmol) was dissolved in 2-propanol (450 mL), resulting in a 250 mM NIPAAm solution; and NIPAAm (25.4 g, 225 mmol) was dissolved in 2-propanol (450 mL), resulting in a 500 mM NIPAAm solution. The NIPAAm solution was deoxygenated using nitrogen gas bubbling for 2 h. Then, CuCl (294 mg, 3.00 mmol), CuCl<sub>2</sub> (45.8 mg, 300 µmol), and Me<sub>6</sub>TREN

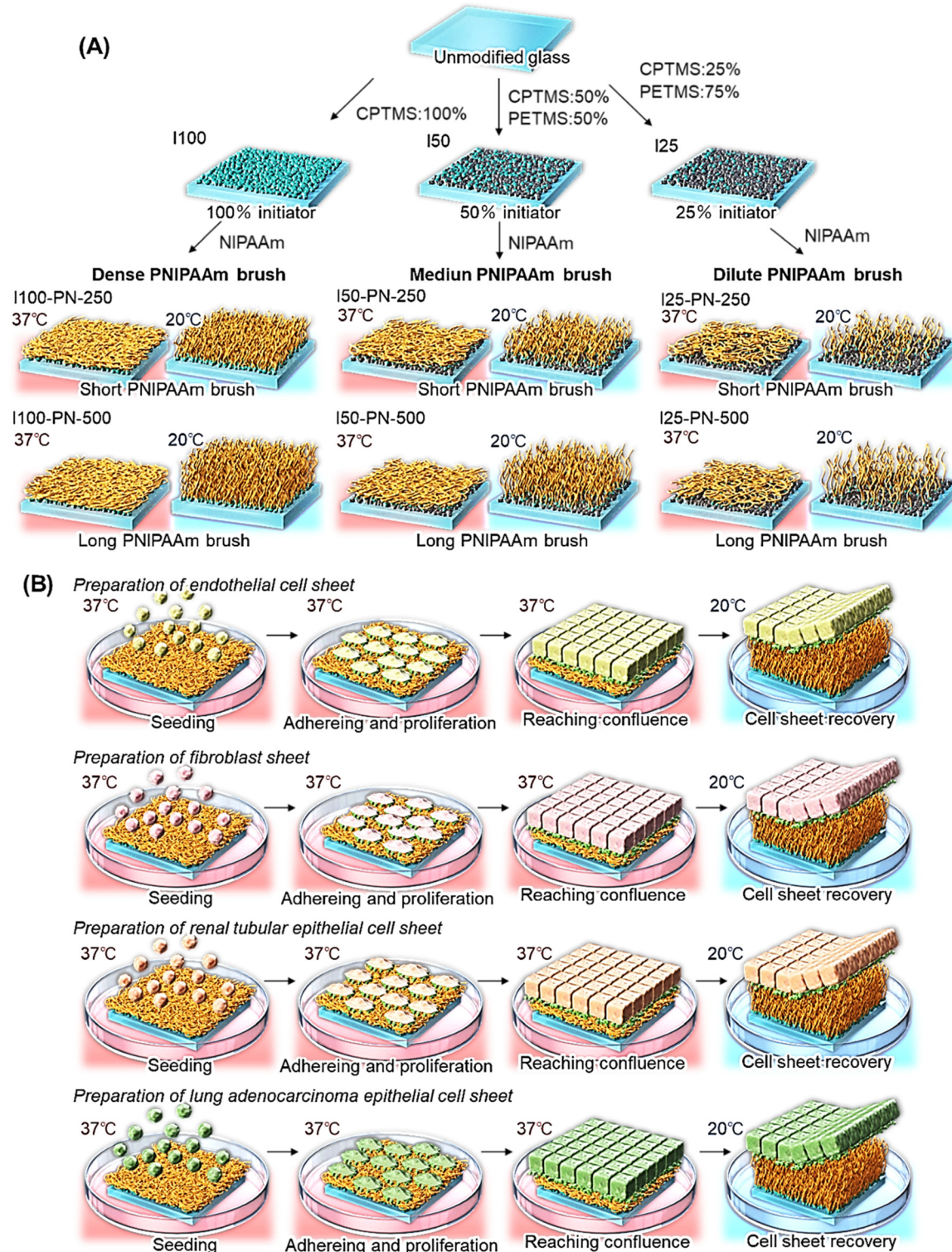


**Fig. 1** Schematic illustrations of the (A) preparation of PNIPAAm brushes with various densities and chain lengths, and (B) preparation of various types of cell sheet with PNIPAAm brushes. CPTMS, (chloromethyl)phenylethyl-trimethoxysilane; PETMS, phenethyltrimethoxysilane; PNIPAAm, poly(*N*-isopropylacrylamide); NIPAAm, *N*-isopropylacrylamide.

(766 mg, 3.30 mmol) were dissolved in NIPAAm solution under nitrogen gas. The ATRP initiator-modified glasses were placed in a glass holder, which was placed in a separable flask.

The glass contained a separable flask, and the ATRP reaction solution was placed in a glove box. The oxygen in the glove box was removed by vacuuming and flushing with nitrogen gas

thrice. The ATRP solution was poured into a separable flask. ATRP was conducted at 25 °C for 16 h. After the reaction, the glass was rinsed with acetone, methanol, and 50 mM aqueous EDTA. The glass was dried at 50 °C for 3 h in a drying oven. The prepared PNIPAAm brush-modified glasses are denoted as I100-PN-X, I50-PN-X, and I25-PN-X, where X is the PNIPAAm monomer concentration.

## 2.2. Characterization of thermoresponsive polymer brushes

The prepared PNIPAAm brushes were characterized using X-ray photoelectron spectroscopy (XPS), attenuated total reflection Fourier transform infrared spectroscopy (ATR/FTIR), contact angle measurements, and fibronectin adsorption observations.

Surface elemental analyses of the prepared PNIPAAm brushes were conducted using XPS (Quantera SXM, Physical Electronics, Chanhassen, MN, USA). Excitation X-rays were produced from a monochromatic AlK $\alpha_{1,2}$  source. XPS analysis with small take off angle can detect the outermost layer of PNIPAAm brush-grafted glass substrate, whereas XPS analysis with large take off angle tends to detect the deep layer of PNIPAAm brush-grafted substrate, leading to the detect of basal glass.<sup>76,77</sup> Thus, we measured XPS with a small take off angle 15° for the detection of the outermost layer of PNIPAAm brush-grafted glass substrate. Deconvolution of the C 1s peak was conducted to determine the composition of the carbon chemical bonds.

The amount of PNIPAAm on glass surfaces was estimated using ATR/FTIR. The FTIR spectrum of the PNIPAAm brush-grafted glass was obtained using an FTIR spectrometer (PerkinElmer, Waltham, MA, USA). The ratio of the peak intensities ( $I_{1650}/I_{1000}$ ) was obtained because the peak at 1650 cm<sup>-1</sup> was attributed to the carbonyl group of the PNIPAAm amide group and the peak at 1000 cm<sup>-1</sup> was attributed to the Si–O of the basal glass. A calibration curve for determining the amount of PNIPAAm was obtained as follows. A predetermined amount of PNIPAAm was dissolved in 2-propanol, and the solution was cast on glass. The 2-propanol was evaporated in a draft chamber. FTIR spectra of the prepared PNIPAAm cast glasses were obtained. The relationship between the amount of PNIPAAm cast onto the glass and the peak intensity ratio was plotted, resulting in a calibration curve between the peak intensity ratio ( $I_{1650}/I_{1000}$ ) and the amount of PNIPAAm. The three FTIR measurements of PNIPAAm brush-modified glass substrates were conducted, and the amount of PNIPAAm was estimated using the peak intensity ratio. The amount of PNIPAAm was obtained by averaging three measurements.

The wettability of the PNIPAAm brushes was observed using contact angle measurements obtained using the captive-bubble method with a contact angle meter (DSA100S, KRUSS, Hamburg, Germany). PNIPAAm brushes were immersed in water at 20 °C and 37 °C. An air bubble (0.5  $\mu$ L) was placed on the PNIPAAm brush in the water. The water contact angle was determined by subtracting the contact angle of the gas phase from 180°.

To evaluate the cell adhesion properties of the prepared PNIPAAm brushes, fibronectin adsorption behavior on the prepared PNIPAAm brushes was observed because fibronectin is an ECM that contributes to cell adhesion. Rhodamine-labelled fibronectin was used to observe fibronectin adsorption by fluorescence microscopy. Rhodamine-labeled fibronectin solution was prepared using phosphate-buffered saline (PBS) at a concentration of 5  $\mu$ g mL<sup>-1</sup>. The solution (2 mL) was placed on the PNIPAAm brush-grafted glass surfaces, then incubated at 37 °C for 2 h. Then, the fibronectin solution was removed from the PNIPAAm brush-grafted glass, and the PNIPAAm brush-grafted glass was rinsed with PBS three times. The PNIPAAm brushes were observed under a fluorescence microscope (ECLIPSE TE2000-U; Nikon, Tokyo, Japan). The obtained image was analyzed by ImageJ (NIH, Bethesda, MD, USA) and the fluorescent intensity ratio of the PNIPAAm brushes were estimated as the fluorescence intensity of I100 was 1.0.

## 2.3. Cell sheet fabrication using prepared PNIPAAm brushes

The cell sheet fabrication performance of the prepared PNIPAAm brushes was investigated using four cell types: endothelial, NIH/3T3, MDCK, and A549 cells. Culture methods for these cells are described in the ESI.†

First, temperature-dependent endothelial cell adhesion and detachment behavior were observed because the endothelial cells were used for the evaluation of various types of PNIPAAm-modified cell culture dishes.<sup>59,60,62</sup> The PNIPAAm brush-grafted glasses were cut into pieces of 25 × 24 mm. The cut glass was then rinsed with 70% ethanol and dried on a clean bench. The glass was then fixed onto polystyrene dishes with grease. Endothelial cells were seeded onto PNIPAAm brush-grafted dishes at a seeding density of  $2.0 \times 10^4$  cells per cm<sup>2</sup>. Then, the endothelial cells on PNIPAAm brush-grafted glasses were incubated at 37 °C for 24 h in a CO<sub>2</sub> incubator under 5% CO<sub>2</sub>. During incubation, the endothelial cells on the PNIPAAm brushes were observed at predetermined times using a microscope (ECLIPSE TE2000-U). Then, PNIPAAm brush-grafted glass was moved to a CO<sub>2</sub> incubator, which was set at 20 °C, and incubated for 4 h. During incubation, the endothelial cells on the PNIPAAm brushes were observed at predetermined times using a microscope (ECLIPSE TE2000-U).

The endothelial cell sheets were prepared as follows. The PNIPAAm brush-grafted glass was cut into 25 × 24 mm pieces, and the cut glass was sterilized with 70% ethanol. The glass substrate was fixed in a polystyrene dish with grease. Endothelial cells were seeded onto PNIPAAm brush-grafted glass dishes at a seeding density of  $2.0 \times 10^5$  cells per cm<sup>2</sup>. The dishes were incubated at 37 °C for 5 days in a CO<sub>2</sub> incubator under 5% CO<sub>2</sub>. After the endothelial cells reached confluence, the dishes were incubated at 20 °C for 20 min.

NIH/3T3, MDCK, and A549 cell sheets were prepared using the same procedures except that incubation was set at 37 °C and 20 °C. When cell adhesion and proliferation were low, incubation at 37 °C was prolonged. Additionally, when the cell sheet detachment was slow, incubation at 20 °C was prolonged.



### 3. Results and discussion

#### 3.1. Characterization of PNIPAAm brushes

Prepared PNIPAAm brushes were characterized using XPS, ATR/FTIR, contact angle measurement, and fibronectin adsorption.

The surface elemental compositions of the prepared initiator-modified glass and PNIPAAm brushes were investigated using XPS (Table 1). The carbon compositions of the initiator-modified surfaces decreased in the following order: I25 > I50 > I100. This was probably due to the difference in the molecular sizes of CPTMS and PETMS. The molecular weights of CPTMS and PETMS were 274.82 and 226.34, respectively. Thus, during the reaction with CPTMS alone, the number of molecules per unit area was less than that during the reaction with CPTMS and PETMS because the molecular size of CPTMS was larger than that of PETMS. Thus, the carbon coverage of the surface followed this order: I100 < I50 < I25. The chlorine composition of the initiator-modified glasses was small (0.4–0.8), which was because CPTMS contains only one chlorine atom in its molecule, making it difficult to detect chlorine *via* XPS.

The PNIPAAm brush surfaces I100-PN250, I50-PN250, and I25-PN250 exhibited larger carbon and nitrogen contents than did the initiator-modified surfaces I100, I50, and I25. This is because the carbon and nitrogen atoms of the grafted PNIPAAm on the glass were detected using XPS. In contrast, the silicon and oxygen contents of the PNIPAAm brushes were lower than those of the initiator-modified glasses. This is because the Si and O of the basal glass of the PNIPAAm brush-grafted glass were difficult to detect using the grafted PNIPAAm brush layer on the glass.

In the deconvolution of the C 1s peaks, a larger C=O bond was observed in the PNIPAAm brushes than that in the initiator-modified surfaces. This was because the carbonyl bond of PNIPAAm was detected, whereas CPTMS and PETMS did not have a carbonyl bond.

The amount of grafted PNIPAAm on the glass was investigated using ATR/FTIR (Table 2). A larger amount of PNIPAAm

**Table 2** ATR/FTIR characterization of PNIPAAm brushes

Code	Initiator (CPTMS): PETMS	Monomer concentration (mmol L <sup>-1</sup> )	Amount of grafted PNIPAAm <sup>a</sup> (μg cm <sup>-2</sup> )
I100-PN250	100 : 0	250	0.91 ± 0.16
I100-PN500		500	1.65 ± 0.21
I50-PN250	50 : 50	250	1.30 ± 0.17
I50-PN500		500	1.56 ± 0.25
I25-PN250	25 : 75	250	0.83 ± 0.42
I25-PN500		500	0.85 ± 0.11

<sup>a</sup> Amount of grafted PNIPAAm was obtained from the peak intensity ratio ( $I_{1650}/I_{1000}$ ) of PNIPAAm brush-grafted glass substrate. Data are expressed as the mean ± standard deviation of three separate ATR/FTIR measurements.

was observed on the PN-500 surfaces prepared using the 500 mM NIPAAm solution compared with that on the PN-250 surfaces prepared using the 250 mM NIPAAm solution. This is because a high concentration of NIPAAm enhances the polymerization reaction in ATRP, leading to a larger amount of PNIPAAm on the glass at higher concentrations.

A comparison of I100-PN500, I50-PN500, and I25-PN500 showed that the PNIPAAm content decreased in the order of I100-PN500 > I50-PN500 > I25-PN500. This is because the initiator density decreased in the order of I100 > I50 > I25.

In many studies dealing with polymer brushes prepared through ATRP, an unbound initiator was added in the reaction solution of ATRP, and the prepared polymer in the reaction solution from the unbound initiator was used for the estimation of the grafted polymer.<sup>78–80</sup> However, in this study, we did not use an unbound initiator in the reaction for the estimation of chain length, because the unbound initiator would adsorb on the ATRP initiator-modified surface through hydrophobic interaction, preventing initiation and propagation from the modified initiator surface. In addition, sacrificial initiator in the reaction solution consumes the monomer in the reaction solution, which is not suitable for the industrial production of PNIPAAm brushes. From previous reports on the

**Table 1** Elemental analyses of PNIPAAm brushes through X-ray photoelectron spectroscopy at a take-off angle of 15°

Code <sup>a</sup>	Atom (%)					C 1s peak deconvolution (%)				
	C	N	O	Si	Cl	N/C ratio	COO	C=O, >N-C=O	C–O, C–N, C–Cl	CHx, C–C, C=C
I100	43.6	—	35.9	15.7	0.8	—	1	<1	10	89
I50	44.0	1.8	38.3	14.8	0.4	—	3	5	15	77
I25	52.1	—	29.9	14.1	0.7	—	<1	2	11	87
I100-PN250	59.5	6.3	21.4	12.8	—	0.11	<1	10	14	76
I50-PN250	67.4	9.1	17.7	5.8	—	0.14	<1	12	16	72
I25-PN250	64.0	8.8	19.3	6.9	—	0.14	<1	12	18	69
Calcd of PNIPAAm <sup>b</sup>	75.0	12.5	12.5	—	0	0.17				
Calcd of CPTMS <sup>b</sup>	70.6	—	17.6	5.88	5.88	—				
Calcd of PETMS <sup>b</sup>	73.3	—	20.0	6.67	—	—				
Calcd of glass <sup>b</sup>	—	—	66.7	33.3	—	—				

<sup>a</sup> Named based on initiator composition in the silane coupling reaction and NIPAAm concentration in ATRP. <sup>b</sup> Theoretical atomic compositions of PNIPAAm, CPTMS, PETMS, and glass.



**Table 3** Contact angle measurements of PNIPAAm brushes

Code	Initiator (CPTMS) : PETMS	Monomer concentration (mmol L <sup>-1</sup> )	Contact angle <sup>a</sup>			
			37 °C		20 °C	
			Degree	cos $\theta$	Degree	cos $\theta$
I100	100 : 0	—	66.4 ± 1.3	0.40 ± 0.02	65.8 ± 0.6	0.41 ± 0.01
I100-PN250		250	58.7 ± 2.0	0.52 ± 0.03	47.9 ± 1.6	0.67 ± 0.02
I100-PN500		500	55.2 ± 1.4	0.57 ± 0.02	51.7 ± 0.7	0.62 ± 0.01
I50	50 : 50	—	65.2 ± 2.6	0.42 ± 0.04	67.0 ± 3.8	0.39 ± 0.06
I50-PN250		250	57.3 ± 2.8	0.54 ± 0.04	47.9 ± 1.6	0.67 ± 0.02
I50-PN500		500	49.5 ± 2.3	0.65 ± 0.03	49.5 ± 0.8	0.65 ± 0.01
I25	25 : 75	—	67.0 ± 1.3	0.39 ± 0.02	65.2 ± 1.9	0.42 ± 0.03
I25-PN250		250	53.8 ± 2.2	0.59 ± 0.03	48.7 ± 1.5	0.66 ± 0.02
I25-PN500		500	53.8 ± 2.2	0.59 ± 0.03	50.9 ± 2.2	0.63 ± 0.03

<sup>a</sup> Data are expressed as the mean ± standard deviation of six measurements.

relationship between PNIPAAm brush length and amount of PNIPAAm using the unbound initiator<sup>76</sup> and the graft density of PNIPAAm on silica beads prepared under similar ATRP conditions,<sup>65</sup> we estimated PNIPAAm brush length and density of the prepared PNIPAAm brushes (Table S1†).

The wettability of the prepared PNIPAAm brushes was investigated by measuring their contact angles (Table 3). The measured contact angles exhibited small measurement error, as shown by the small standard deviation. The initiator-modified surfaces exhibited hydrophobic properties (large contact angle) compared with those of the PNIPAAm brush-modified surfaces. This was attributed to the hydrophobic properties of the phenyl groups of CPTMS and PETMS and the relatively hydrophilic properties of the grafted PNIPAAm. PNIPAAm brushes exhibited temperature-dependent hydrophobicity change because PNIPAAm brushes become hydrophobic and hydrophilic at 37 °C and 20 °C, respectively. This is because PNIPAAm hydrates and dehydrates at high and low temperatures, respectively. A larger amount of PNIPAAm-grafted brush (PN-500) exhibited relatively high hydrophilicity compared with that of a small amount of PNIPAAm (PN-250). This was because the long PNIPAAm brush tended to hydrate more than the short PNIPAAm brush. Previous reports have indicated that the hydrophobicity of PNIPAAm brushes increases with the length of the PNIPAAm brush because the hydration of PNIPAAm brushes increases with PNIPAAm brush length.<sup>60,61,81,82</sup>

To investigate the protein adsorption properties of the prepared PNIPAAm brushes, rhodamine-labelled fibronectin adsorption was investigated (Fig. 2). Fibronectin is one of the proteins that contribute to cell adhesion of extracellular matrices.<sup>83</sup> Thus, fibronectin adsorption on PNIPAAm brushes reflects the cell adhesion properties. Fluorescent images of the fibronectin-adsorbed PNIPAAm brushes were observed using a fluorescent microscope. Previous reports have suggested that amount of the fluorescent protein can be determined by the fluorescent intensity of the images.<sup>84–86</sup> Thus, the fluorescent intensity ratio was obtained using fluorescent image analysis

of adsorbed PNIPAAm brushes. The quantum yield of rhodamine may be affected by the density of rhodamine. Rhodamine was conjugated to fibronectin, and the rhodamine conjugated fibronectin was adsorbed on the PNIPAAm brush-grafted surfaces. Thus, rhodamine density on the surface was not sufficiently high to affect quantum yield.

The initiator-modified surface (I100) exhibited large adsorption of fibronectin compared with that of the PNIPAAm brushes. This is because the strong hydrophobicity of CPTMS induces significant adsorption of fibronectin (Fig. 2D and F). For the PNIPAAm brushes, larger fibronectin adsorption was observed in the order of I25-PN-250, I50-PN-250, and I100-PN-250 (Fig. 2A–C and F). This is because the low-density PNIPAAm brush, I25-PN-250, exposed PETMS at the graft interface, whereas the dense PNIPAAm brush, I100-PN-250, did not. Exposure to PETMS enhances fibronectin adsorption. Thus, fibronectin adsorption was enhanced by decreasing the amount of PNIPAAm brushes. These results indicated that dilute PNIPAAm brushes have increased cell adhesion activity, which can be attributed to enhanced ECM adsorption.

### 3.2. Endothelial cell adhesion on PNIPAAm brushes

The cell adhesion properties of the prepared PNIPAAm brushes were investigated by observing temperature-dependent endothelial cell adhesion behaviors (Fig. 3).

The short, dense PNIPAAm brush, I100-PN-250, exhibited endothelial adhesion after incubation at 37 °C for 24 h. Then, at a reduced temperature of 20 °C, endothelial cells detached from the I100-PN-250 brush. This is because of PNIPAAm dehydration and hydration at 37 °C and 20 °C, respectively. Endothelial cells adhered to the PNIPAAm brush at 37 °C because PNIPAAm dehydrated at 37 °C, and the hydrophobicity of the dehydrated PNIPAAm brush was suitable for adhesion of endothelial cells. On the contrary, PNIPAAm hydrates and becomes hydrophilic at 20 °C, and endothelial cells do not tend to adhere to the PNIPAAm brush.

In contrast, the long, dense PNIPAAm brush, I100-PN-500, was scarcely adhered to by endothelial cells after incubation at



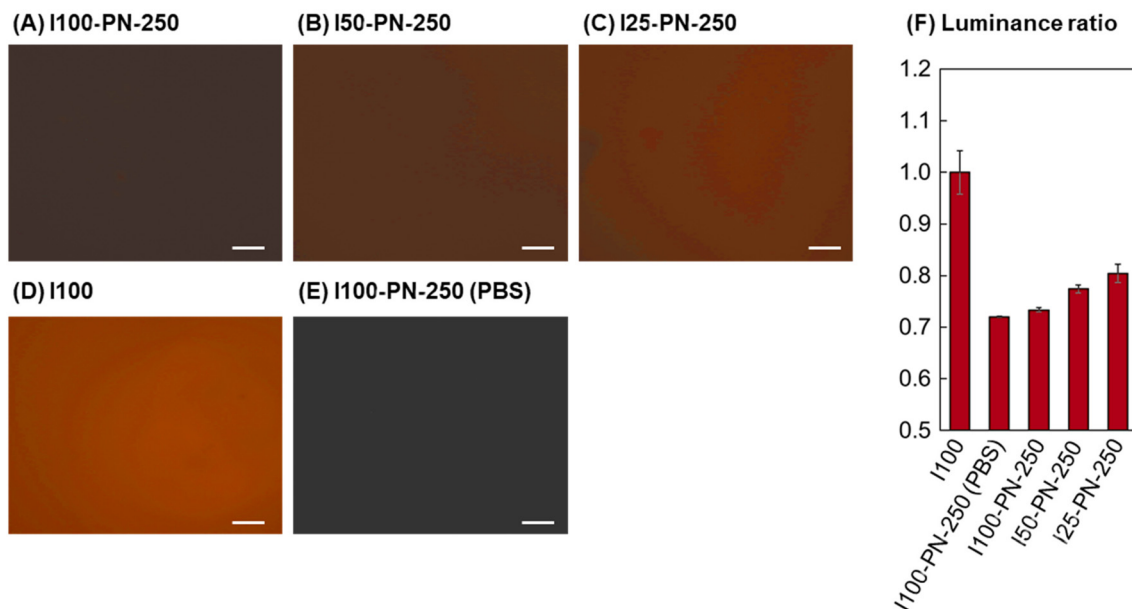


**Fig. 2** Fibronectin adsorption on prepared PNIPAAm brushes. (A)–(E) Fluorescent microscopic images of rhodamine-labelled fibronectin adsorbed to PNIPAAm brush surfaces at 37 °C. Scale bar: 100  $\mu$ m. (F) Luminance ratio of fibronectin-adsorbed PNIPAAm brushes.

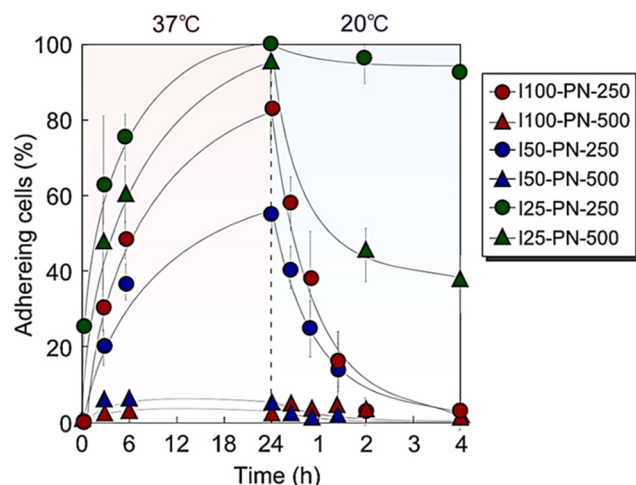


**Fig. 3** Endothelial cell adhesion and detachment profile on PNIPAAm brushes.

37 °C for 24 h. This is because of the relatively hydrophilic properties of long PNIPAAm brushes. Previous reports have indicated that long PNIPAAm brushes tend to be hydrophilic because PNIPAAm mobility increases with increasing length, leading to enhanced hydration.<sup>60,81,82</sup> The hydrophilic property of the long PNIPAAm brush resulted in low ECM adsorption, leading to cell-repulsive properties even at high temperatures. These results indicate that long PNIPAAm brushes are not suitable for endothelial adhesion at 37 °C.

The short, moderate-density PNIPAAm brush (I50-PN-250) exhibited endothelial cell adhesion. The adhesion ratio of the endothelial cells was relatively low compared with that of I100-

PN-250. This was probably due to the relatively long PNIPAAm chain of I50-PN-250 compared with that of I100-PN-250. A previous report indicated that a dilute PNIPAAm brush using 50% initiator density had a relatively long PNIPAAm length (19 600) compared with that of a dense PNIPAAm brush using 100% initiator density (11 300).<sup>65</sup> Thus, I50-PN-250 has a relatively long PNIPAAm chain, leading to lower cell adhesion compared with that of I100-PN-250.

I50-PN-500 exhibited a low cell adhesion ratio owing to its hydrophilic properties. The long PNIPAAm brushes tended to hydrate because of the increased mobility of PNIPAAm, leading to the low cell adhesion of I50-PN-500.

At 37 °C, I25-PN-250 and I25-PN-500 exhibited a high endothelial cell adhesion rate. This is because the PNIPAAm densities of I25-PN-250 and I25-PN-500 were low, and hydrophobic PETMS was exposed at the graft interfaces, which enhanced ECM adsorption and subsequent cell adhesion. A previous report indicated that a dilute PNIPAAm brush prepared using PETMS exhibited strong hydrophobicity compared with that of a dense PNIPAAm brush, resulting in strong hydrophobic interaction with steroids.<sup>87</sup> Likewise, PETMS in dilute PNIPAAm brushes, I25-PN-250 and I25-PN-500, induced ECM adsorption and subsequent endothelial cell adhesion at 37 °C. At a reduced temperature of 20 °C, I25-PN-250 scarcely demonstrated detachment of endothelial cells, and a small ratio of cell detachment was observed in I25-PN-250.

Using the I100-PN-250 brush, an endothelial cell sheet was prepared (Fig. 4). Endothelial cells were seeded to the I100-PN-250 brush and incubated at 37 °C for 5 days. The cells proliferated on the PNIPAAm brushes and reached confluence (Fig. 4A). At a reduced temperature of 20 °C, the endothelial cell sheets were detached from the I100-PN-250 brush (Fig. 4B)

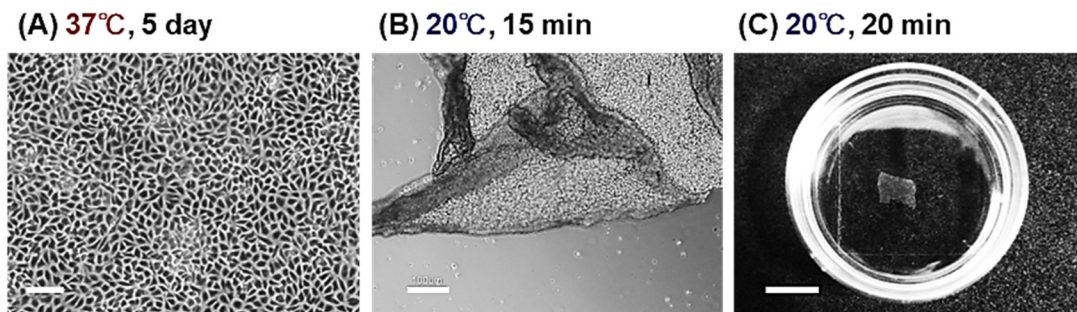


**Fig. 4** Morphologies of endothelial cells on PNIPAAm brush surfaces (I100-PN-250) at (A) 37 °C after 5 days incubation (scale bar: 100  $\mu$ m), (B) 20 °C after 15 min incubation (scale bar: 100  $\mu$ m), and (C) 20 °C after 20 min incubation (scale bar: 10 mm).

and C). This characteristic is attributed to the temperature-dependent change in the hydrophobicity of the PNIPAAm brush. At 37 °C, PNIPAAm brushes became hydrophobic, and endothelial cells could adhere to them. These endothelial cells proliferated and reached confluence. At a reduced temperature of 20 °C, the PNIPAAm brushes hydrated, and the adhered confluent cells detached.

Endothelial cells adhered, proliferated, and reached confluence on the dilute PNIPAAm brushes (I25-PN-250 and I25-PN-500). However, the endothelial cell sheets could not be detached from the PNIPAAm brushes at 20 °C, because the strong hydrophobic PETMS in the dilute PNIPAAm brushes maintained the adsorption of ECM and cell adhesion, even in the presence of PNIPAAm hydration.

Endothelial cells adhered to the moderate-density PNIPAAm brushes (I50-PN-250 and I50-PN-500). However, endothelial cells did not proliferate until confluence. This was attributed to the relatively long PNIPAAm brushes, I50-PN-250 and I50-PN-500, which were relatively hydrophilic. Thus, endothelial cells tended to detach, did not proliferate, and did not reach confluence.

Viability of the cell sheet should be maintained for effective therapy using the recovered cell sheet. Previous reports indicated that recovered cells from PNIPAAm brushes exhibited viability after temperature reduction.<sup>88–91</sup> Thus, the viability of recovered cell sheets from PNIPAAm brushes is maintained after temperature reduction.

### 3.3. Various types of cell sheet preparation with PNIPAAm brushes

PNIPAAm brushes were investigated for cell sheet fabrication for various cell types. NIH/3T3 cell sheets were prepared using six types of PNIPAAm brushes (Fig. 5). NIH/3T3 cells adhered and proliferated at 37 °C for 4 days on I100-PN-250. At a reduced temperature of 20 °C, the cell sheet was not detached. This is probably because NIH/3T3 cells have strong adhesion properties, leading to adhesion even in hydrated PNIPAAm brushes.

I100-PN-500 also exhibited NIH/3T3 cell adhesion and proliferation at 37 °C. After 4 days of incubation with proliferation of NIH/3T3 cells, the NIH/3T3 cells reached confluence. This tendency differs from that of endothelial cells, which did not

adhere to I100-PN-500 because of the relatively hydrophilic nature of the longer PNIPAAm brushes. In contrast, the NIH/3T3 cells adhered to I100-PN-500 because of the strong adhesion properties of NIH/3T3 cells. At a reduced temperature of 20 °C, the NIH/3T3 cell sheet detached from the I100-PN-500 brushes. These results indicate that NIH/3T3 cell sheets can be prepared using the I100-PN-500 brush.

On the moderate density PNIPAAm brush with short PNIPAAm chain length, I50-PN-250 exhibited NIH/3T3 cell adhesion at 37 °C. After 4 days of incubation, the NIH/3T3 cells reached confluence. At a reduced temperature of 20 °C, the NIH/3T3 cell sheet was recovered from I50-PN-250. These results indicate that I50-PN-250 is suitable for NIH/3T3 cell sheet preparation, similar to I100-PN-500.

On I50-PN-500, NIH/3T3 cells did not adhere at 37 °C owing to the hydrophilicity of I50-PN-500, which was attributed to its relatively long PNIPAAm chains.

I25-PN-250 exhibited NIH/3T3 adhesion and proliferation at 37 °C. NIH/3T3 cells reached confluence after 4 days of incubation. However, the NIH/3T3 sheet was not detached from I25-PN-250 at a reduced temperature of 20 °C. This is because the strong hydrophobicity of the PETMS exposed on the I25-PN-250 interfaces retained the adhesion of NIH/3T3 through the adsorbed ECM even during the hydration of PNIPAAm.

The I25-PN-500 adhered to NIH/3T3 cells at 37 °C, leading to proliferation and confluence after 4 days. The NIH/3T3 cell sheet detached from the I25-PN-500 after the temperature was changed to 20 °C. This is because the relatively long PNIPAAm brush of I25-PN-500 could demonstrate detachment of the NIH/3T3 cell sheet compared with that of I25-PN-250.

These results indicate that NIH/3T3 cell sheets can be prepared using the three types of PNIPAAm brushes: I100-PN-500, I50-PN-250, and I25-PN-500.

MDCK cell sheets were prepared using the prepared PNIPAAm brushes (Fig. 6). I100-PN-250, I25-PN-250, and I25-PN-500 exhibited MDCK cell adhesion, proliferation, and confluence at 37 °C (Fig. 6A-1, E-1 and F-1). However, after changing the temperature to 20 °C, the MDCK cell sheet did not detach because the hydration of the PNIPAAm brush was not sufficient.

In contrast, MDCK cells did not adhere to I50-PN-500 because the hydrophobic properties of the PNIPAAm brush were not sufficient, even in the dehydrated state of PNIPAAm.



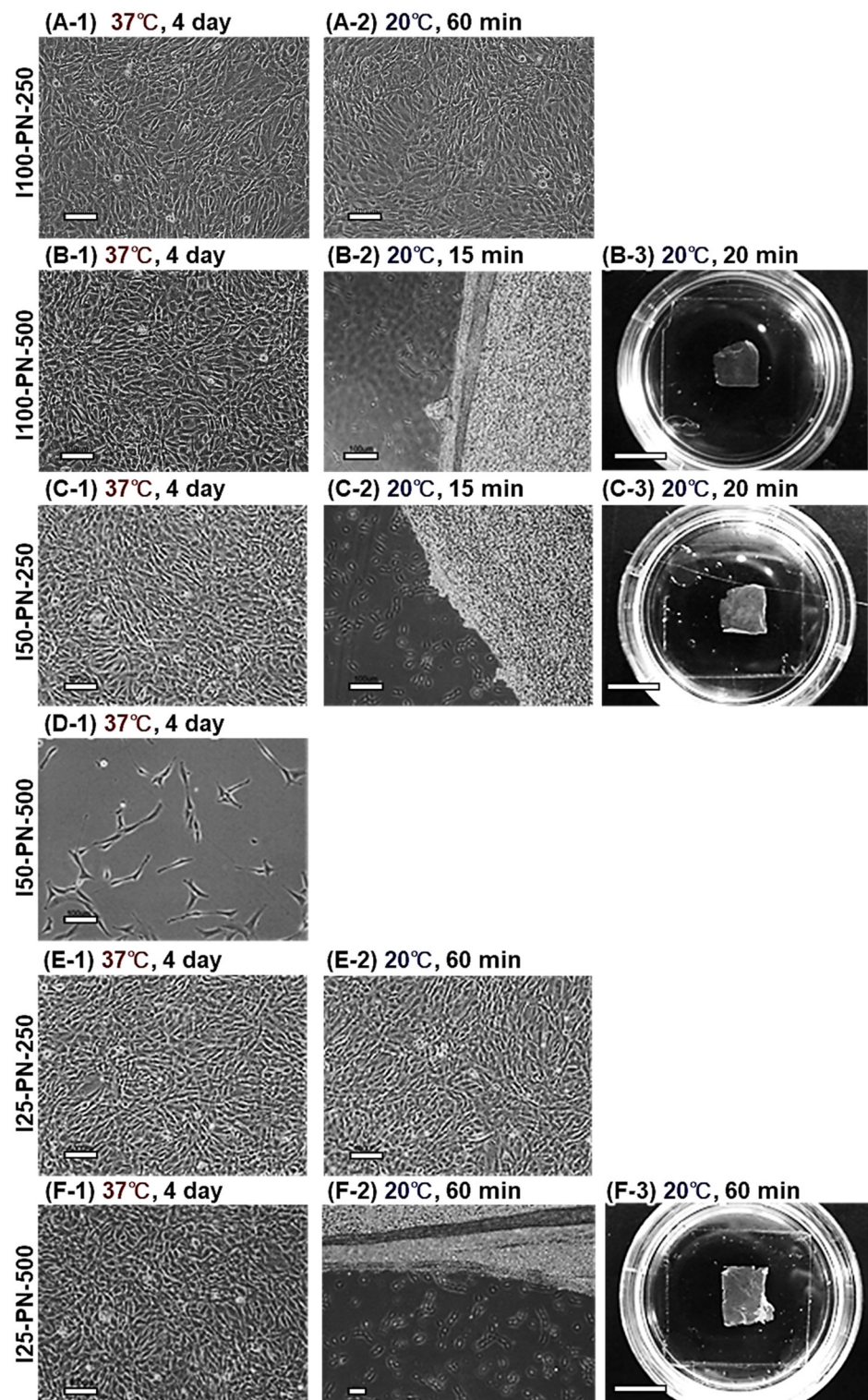


**Fig. 5** Morphologies of NIH/3T3 on PNIPAAm brush surfaces. (A) I100-PN-250, (B) I100-PN-500, (C) I50-PN-250, (D) I50-PN-500, (E) I25-PN-250, and (F) I25-PN-500. Incubation at 37 °C and subsequent incubation at 20 °C. Scale bars: 100  $\mu$ m (−1 and −2) and 10 mm (−3).

Furthermore, the MDCK cells adhered to I100-PN-500 and I50-PN-250 in an aggregated form. However, MDCK cells became confluent even after 8 days of incubation at 37 °C (Fig. 6B-1 and C-1). The strong intercellular adhesion of MDCK cells pre-

vented cell proliferation on the highly hydrophilic surface, which was difficult for cells to adhere to.

These results indicate that it is difficult to prepare MDCK cell sheets using PNIPAAm brushes because MDCK cells do not

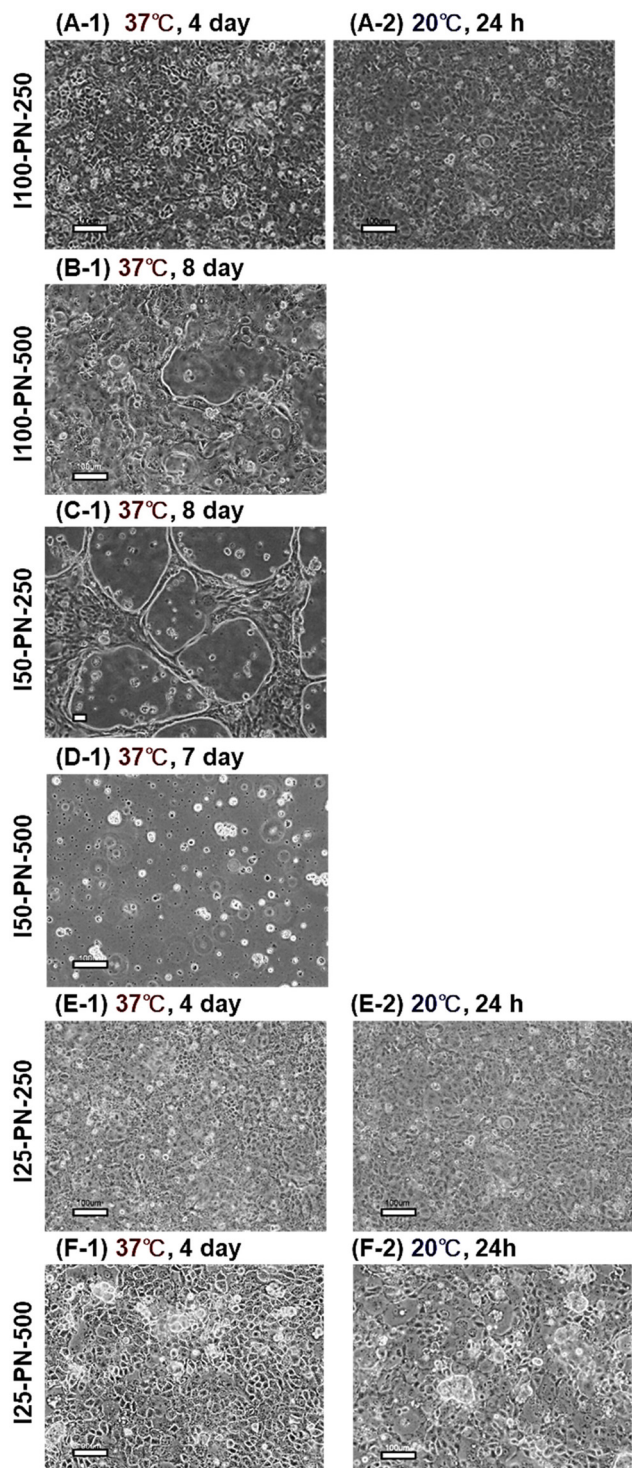


**Fig. 6** Morphologies of MDCK on PNIPAAm brush surfaces. (A) I100-PN-250, (B) I100-PN-500, (C) I50-PN-250, (D) I50-PN-500, (E) I25-PN-250, and (F) I25-PN-500. Incubation at 37 °C and subsequent incubation at 20 °C. Scale bars: 100  $\mu$ m in (−1) and (−2).

adhere or proliferate on the relatively hydrophobic brush, or adhere but do not detach from the relatively hydrophobic PNIPAAm brush at 20 °C.

A549 cell sheet preparation was investigated using the prepared PNIPAAm brushes (Fig. 7). A549 cells adhered and proliferated on I100-PN-500 and I50-PN-250 at 37 °C. After 4 days of incubation, the A549 cells reached confluence (Fig. 7B-1 and C-1). At a reduced temperature of 20 °C, the A549 cell sheet was successfully recovered (Fig. 7B-3 and C-3). However, a defect was observed at the edge of the A549 cell sheet prepared using I100-PN-500, probably because the cell-cell junctions of A549 cells were relatively weak.

I100-PN-250, I25-PN-250, and I25-PN-500 exhibited A549 adhesion and proliferation, reaching confluence after 4 days of incubation at 37 °C. However, the A549 cell sheet was not detached at a reduced temperature of 20 °C. This is because the hydrophilicity of I100-PN-250, I25-PN-250, and I25-PN-500 at 20 °C is not adequate for the detachment of the A549 cell sheet. The EC sheet detached from I100-PN-250 at 20 °C. Thus, A549 adhesion on I100-PN-250 was strong compared with that of EC, indicating that A549 cells have strong cell adhesivity compared with that of EC. A549 cells did not adhere to, or proliferate on I50-PN-500, even at 37 °C, because the hydrophobic properties of the I50-PN-500 were insufficient for the continuous adhesion and proliferation of A549 cells.

These results indicate that A549 cell sheets can be prepared using I100-PN-500 and I50-PN-250 brushes. However, such cell sheets are fragile, probably because of weak cell-cell junctions.

The four types of cell sheets prepared using the prepared PNIPAAm brushes are summarized in Table 4.

The cell sheet preparation performance varied with cell type, and with PNIPAAm brush density and length. Endothelial cell sheets were prepared using I100-PN-250. The three types of PNIPAAm brushes (I100-PN-500, I50-PN-250, and I50-PN-500) did not demonstrate adherence of endothelial cells because of the relatively hydrophilic nature of the PNIPAAm brush, which was attributed to the relatively long PNIPAAm chain. In contrast, endothelial cells adhered to dilute PNIPAAm brushes at 37 °C. However, the endothelial cells did not detach, which was attributed to the strong hydrophobicity of the exposed PETMS.

NIH/3T3 cell sheets were prepared using three types of PNIPAAm brushes: I100-PN-500, I50-PN-250, and I25-PN-500. Owing to the relatively good adhesive properties of NIH/3T3 cells, NIH/3T3 cell sheets could be prepared using various types of PNIPAAm brushes, whereas endothelial cell sheets could be prepared using only one type of PNIPAAm brush: I100-PN-250.

In contrast, MDCK cell sheets could not be prepared using any of the six types of PNIPAAm brush. Previous reports have indicated that PNIPAAm-modified cell culture dishes prepared using EB irradiation can be used to prepare MDCK cell sheets. Thus, PNIPAAm-modified dish-prepared EB irradiation is more suitable than are PNIPAAm brushes for preparing MDCK cell sheets.

A549 cell sheets were prepared using two types of PNIPAAm brush: I100-PN-500 and I50-PN-250. The prepared A549 cell sheets had a fragile structure attributed to weak cell-cell junctions.



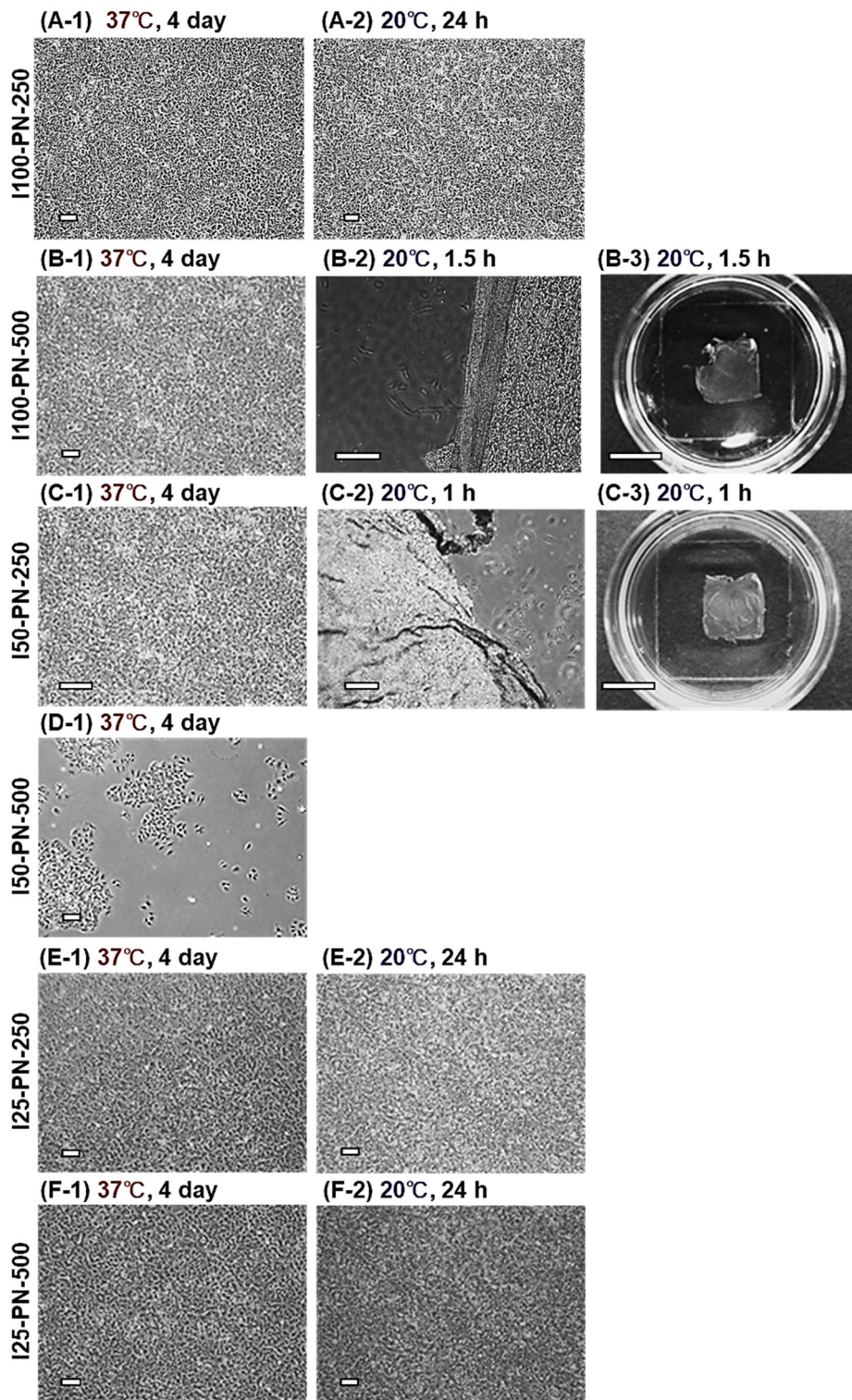


**Fig. 7** Morphologies of A549 on PNIPAAm brush surfaces. (A) I100-PN-250, (B) I100-PN-500, (C) I50-PN-250, (D) I50-PN-500, (E) I25-PN-250, and (F) I25-PN-500. Incubation at 37 °C and subsequent incubation at 20 °C. Scale bars: 100  $\mu$ m in (–1 and –2) and 10 mm.

These results demonstrate that the cell adhesion and cell sheet detachment properties of PNIPAAm brushes can be modulated by changing the PNIPAAm graft density and chain length. The appropriate PNIPAAm brush conditions

for the cell sheet preparation varied depending on cell type. Thus, modulation of PNIPAAm brush density and length is an effective approach for preparing target cell sheets.



**Table 4** Adhesion and detachment behavior of various cell types and cell sheet harvests on PNIPAAm brush surfaces

Code	EC			NIH/3T3			MDCK			A549		
	37 °C	20 °C	Cell sheet preparation	37 °C	20 °C	Cell sheet preparation	37 °C	20 °C	Cell sheet preparation	37 °C	20 °C	Cell sheet preparation
I100-PN-250	A	D	P	A	A	NP	A	A	NP	A	A	NP
I100-PN-500	NA	—	NP	A	D	P	A/NC	—	NP	A	D	P
I50-PN-250	NA	—	NP	A	D	P	A/NC	—	NP	A	D	P
I50-PN-500	NA	—	NP	NA	—	NP	NA	—	NP	NA	—	NP
I25-PN-250	A	A	NP	A	A	NP	A	A	NP	A	A	NP
I25-PN-500	A	A	NP	A	D	P	A	A	NP	A	A	NP

A: adhered, NA: not adhered, D: detached, P: prepared, NP: not prepared, NC: not confluent.

## 4. Conclusions

We investigated the cell sheet preparation performance of PNIPAAm brushes with various densities and chain lengths using four types of cells. PNIPAAm brush-grafted glasses were prepared by silanization and subsequent ATRP. The density of the PNIPAAm brushes was modulated by changing the initiator composition, and the PNIPAAm brush length was modulated by changing the monomer concentration in the ATRP. The hydrophilicity of the PNIPAAm brushes increased with increasing PNIPAAm brush length because the long PNIPAAm brushes tended to hydrate. Fibronectin adsorption increased with decreasing PNIPAAm density. This is because the exposed hydrophobic PETMS in the dilute PNIPAAm brush enhanced the adsorption of fibronectin. The cell-sheet fabrication ability was investigated using six types of PNIPAAm brush. The endothelial cell sheet was fabricated using only a dense, short PNIPAAm brush. NIH/3T3 sheets were fabricated using three types of PNIPAAm brush: a dense and long PNIPAAm brush, moderate-density and short PNIPAAm brush, and dilute and long PNIPAAm brush. MDCK cell sheets could not be prepared using the PNIPAAm brushes. A549 cell sheets were prepared using a dense and short PNIPAAm brush and moderately short PNIPAAm brush. These results indicate that the optimal PNIPAAm brush conditions for cell sheet preparation vary depending on cell type. Thus, modulation of PNIPAAm brush density and length is an effective approach for preparing target cell sheets.

## Author contributions

Kenichi Nagase: Conceptualization, methodology, investigation, writing—original draft writing—review & editing, supervision. Minami Watanabe: Methodology, investigation. Akihiko Kikuchi: Conceptualization, writing—review & editing, supervision. Teruo Okano: Writing—review & editing, supervision.

## Data availability

Data are available from the corresponding author upon reasonable request.

## Conflicts of interest

A. K. and T. O. are investors in CellSeed. T. O. is an inventor/developer with a patent for temperature-responsive culture surfaces.

## Acknowledgements

This study was supported by Grants-in-Aid for Scientific Research from the Japan Society for the Promotion of Science (JP21KK0199, JP22K19899, and JP24K01181), the Precise Measurement Technology Promotion Foundation (PMTP-F), and the CASIO Science Promotion Foundation.

## References

- 1 R. Langer and J. Vacanti, *Science*, 1993, **260**, 920–926.
- 2 T. Shin'oka, Y. Imai and Y. Ikada, *N. Engl. J. Med.*, 2001, **344**, 532–533.
- 3 K. Nishida, M. Yamato, Y. Hayashida, K. Watanabe, K. Yamamoto, E. Adachi, S. Nagai, A. Kikuchi, N. Maeda, H. Watanabe, T. Okano and Y. Tano, *N. Engl. J. Med.*, 2004, **351**, 1187–1196.
- 4 T. Iwata, M. Yamato, K. Washio, T. Yoshida, Y. Tsumanuma, A. Yamada, S. Onizuka, Y. Izumi, T. Ando, T. Okano and I. Ishikawa, *Regener. Ther.*, 2018, **9**, 38–44.
- 5 M. Sato, M. Yamato, G. Mitani, T. Takagaki, K. Hamahashi, Y. Nakamura, M. Ishihara, R. Matoba, H. Kobayashi, T. Okano, J. Mochida and M. Watanabe, *npj Regener. Med.*, 2019, **4**, 4.



6 N. Yamada, T. Okano, H. Sakai, F. Karikusa, Y. Sawasaki and Y. Sakurai, *Makromol. Chem., Rapid Commun.*, 1990, **11**, 571–576.

7 T. Okano, N. Yamada, M. Okuhara, H. Sakai and Y. Sakurai, *Biomaterials*, 1995, **16**, 297–303.

8 T. Okano, N. Yamada, H. Sakai and Y. Sakurai, *J. Biomed. Mater. Res.*, 1993, **27**, 1243–1251.

9 A. Kushida, M. Yamato, C. Konno, A. Kikuchi, Y. Sakurai and T. Okano, *J. Biomed. Mater. Res.*, 1999, **45**, 355–362.

10 A. Kushida, M. Yamato, A. Kikuchi and T. Okano, *J. Biomed. Mater. Res.*, 2001, **54**, 37–46.

11 Y. Sawa, S. Miyagawa, T. Sakaguchi, T. Fujita, A. Matsuyama, A. Saito, T. Shimizu and T. Okano, *Surg. Today*, 2012, **42**, 181–184.

12 T. Ohki, M. Yamato, M. Ota, R. Takagi, D. Murakami, M. Kondo, R. Sasaki, H. Namiki, T. Okano and M. Yamamoto, *Gastroenterology*, 2012, **143**, 582–588.

13 K. Yamamoto, M. Yamato, T. Morino, H. Sugiyama, R. Takagi, Y. Yaguchi, T. Okano and H. Kojima, *npj Regener. Med.*, 2017, **2**, 6.

14 M. Kanzaki, R. Takagi, K. Washio, M. Kokubo and M. Yamato, *npj Regener. Med.*, 2017, **2**, 26.

15 Y. Haraguchi, T. Shimizu, T. Sasagawa, H. Sekine, K. Sakaguchi, T. Kikuchi, W. Sekine, S. Sekiya, M. Yamato, M. Umezu and T. Okano, *Nat. Protocols*, 2012, **7**, 850–858.

16 H. Sekine, T. Shimizu, K. Sakaguchi, I. Dobashi, M. Wada, M. Yamato, E. Kobayashi, M. Umezu and T. Okano, *Nat. Commun.*, 2013, **4**, 1399.

17 K. Kim, R. Utoh, K. Ohashi, T. Kikuchi and T. Okano, *J. Tissue Eng. Regener. Med.*, 2017, **11**, 2071–2080.

18 K. Sakaguchi, T. Shimizu, S. Horaguchi, H. Sekine, M. Yamato, M. Umezu and T. Okano, *Sci. Rep.*, 2013, **3**, 1316.

19 M. Heskins and J. E. Guillet, *J. Macromol. Sci., Part A: Pure Appl. Chem.*, 1968, **2**, 1441–1455.

20 A. Halperin, M. Kröger and F. M. Winnik, *Angew. Chem., Int. Ed.*, 2015, **54**, 15342–15367.

21 J. Akimoto, M. Nakayama, K. Sakai and T. Okano, *Mol. Pharm.*, 2010, **7**, 926–935.

22 Y. Hiruta, Y. Kanda, N. Katsuyama and H. Kanazawa, *RSC Adv.*, 2017, **7**, 29540–29549.

23 K. Nagase, M. Hasegawa, E. Ayano, Y. Maitani and H. Kanazawa, *Int. J. Mol. Sci.*, 2019, **20**, 430.

24 R. Nemoto, K. Fujieda, Y. Hiruta, M. Hishida, E. Ayano, Y. Maitani, K. Nagase and H. Kanazawa, *Colloids Surf., B*, 2019, **176**, 309–316.

25 G.-F. Luo, W.-H. Chen and X.-Z. Zhang, *ACS Macro Lett.*, 2020, **9**, 872–881.

26 M. Maekawa-Matsuura, K. Fujieda, Y. Maekawa, T. Nishimura, K. Nagase and H. Kanazawa, *ACS Omega*, 2019, **4**, 6443–6451.

27 N. L. Eremeev and A. V. Kukhtin, *Anal. Chim. Acta*, 1997, **347**, 27–34.

28 T. Mori and M. Maeda, *Langmuir*, 2004, **20**, 313–319.

29 M. R. Islam, S. Xie, D. Huang, K. Smyth and M. J. Serpe, *Anal. Chim. Acta*, 2015, **898**, 101–108.

30 M. Islam, A. Ahiabu, X. Li and M. Serpe, *Sensors*, 2014, **14**, 8984.

31 Y. Hiruta, M. Shimamura, M. Matsuura, Y. Maekawa, T. Funatsu, Y. Suzuki, E. Ayano, T. Okano and H. Kanazawa, *ACS Macro Lett.*, 2014, **3**, 281–285.

32 M. Ebara, J. M. Hoffman, A. S. Hoffman and P. S. Stayton, *Lab Chip*, 2006, **6**, 843–848.

33 J. M. Hoffman, P. S. Stayton, A. S. Hoffman and J. J. Lai, *Bioconjugate Chem.*, 2015, **26**, 29–38.

34 K. Nagase, *Anal. Sci.*, 2024, **40**, 827–841.

35 Y.-J. Kim, S. H. Kim, T. Fujii and Y. T. Matsunaga, *Biomater. Sci.*, 2016, **4**, 953–957.

36 M. Matsuura, M. Ohshima, Y. Hiruta, T. Nishimura, K. Nagase and H. Kanazawa, *Int. J. Mol. Sci.*, 2018, **19**, 1646.

37 Y. Hiruta, *Polym. J.*, 2022, **54**, 1419–1430.

38 Y. Maekawa, N. Okamoto, Y. Okada, K. Nagase and H. Kanazawa, *Sci. Rep.*, 2020, **10**, 8828.

39 K. Nagase and H. Kanazawa, *Anal. Chim. Acta*, 2020, **1138**, 191–212.

40 E. Ayano and H. Kanazawa, *J. Sep. Sci.*, 2006, **29**, 738–749.

41 Y. Maekawa, E. Ayano, K. Nagase and H. Kanazawa, *Anal. Sci.*, 2021, **37**, 651–660.

42 K. Nagase, G. Edatsune, Y. Nagata, J. Matsuda, D. Ichikawa, S. Yamada, Y. Hattori and H. Kanazawa, *Biomater. Sci.*, 2021, **9**, 7054–7064.

43 Y. Maekawa, K. Yamazaki, M. Ihara, K. Nagase and H. Kanazawa, *Anal. Bioanal. Chem.*, 2020, **412**, 5341–5351.

44 K. Okubo, K. Ikeda, A. Oaku, Y. Hiruta, K. Nagase and H. Kanazawa, *J. Chromatogr. A*, 2018, **1568**, 38–48.

45 K. Nagase, S. Ishii, A. Takeuchi and H. Kanazawa, *Sep. Purif. Technol.*, 2022, **299**, 121750.

46 K. Nagase, S. Kitazawa, T. Kogure, S. Yamada, K. Katayama and H. Kanazawa, *Sep. Purif. Technol.*, 2022, **286**, 120445.

47 K. Nagase, K. Yamazaki, Y. Maekawa and H. Kanazawa, *Mater. Today Bio*, 2023, **18**, 100521.

48 K. Komori, M. Udagawa, M. Shinohara, K. Montagne, T. Tsuru and Y. Sakai, *Biomater. Sci.*, 2013, **1**, 510–518.

49 M. Yamato, Y. Akiyama, J. Kobayashi, J. Yang, A. Kikuchi and T. Okano, *Prog. Polym. Sci.*, 2007, **32**, 1123–1133.

50 H. M. El-Husseiny, E. A. Mady, L. Hamabe, A. Abugomaa, K. Shimada, T. Yoshida, T. Tanaka, A. Yokoi, M. Elbadawy and R. Tanaka, *Mater. Today Bio*, 2022, **13**, 100186.

51 K. Nagase, M. Nagaoka, Y. Nakano and R. Utoh, *J. Controlled Release*, 2024, **366**, 160–169.

52 M. E. Nash, D. Healy, W. M. Carroll, C. Elvira and Y. A. Rochev, *J. Mater. Chem.*, 2012, **22**, 19376–19389.

53 M. A. Cooperstein and H. E. Canavan, *Langmuir*, 2010, **26**, 7695–7707.

54 K. Mokhtarinia and E. Masaeli, *Eur. Polym. J.*, 2020, **141**, 110076.

55 F. Doberenz, K. Zeng, C. Willems, K. Zhang and T. Groth, *J. Mater. Chem. B*, 2020, **8**, 607–628.

56 K. Nagase, M. Yamato, H. Kanazawa and T. Okano, *Biomaterials*, 2018, **153**, 27–48.



57 J. Kobayashi, A. Kikuchi, T. Aoyagi and T. Okano, *J. Biomed. Mater. Res., Part A*, 2019, **107**, 955–967.

58 K. Nagase, *Adv. Colloid Interface Sci.*, 2021, **295**, 102487.

59 Y. Akiyama, A. Kikuchi, M. Yamato and T. Okano, *Langmuir*, 2004, **20**, 5506–5511.

60 A. Mizutani, A. Kikuchi, M. Yamato, H. Kanazawa and T. Okano, *Biomaterials*, 2008, **29**, 2073–2081.

61 K. Nagase, M. Watanabe, A. Kikuchi, M. Yamato and T. Okano, *Macromol. Biosci.*, 2011, **11**, 400–409.

62 H. Takahashi, M. Nakayama, M. Yamato and T. Okano, *Biomacromolecules*, 2010, **11**, 1991–1999.

63 H. Takahashi, N. Matsuzaka, M. Nakayama, A. Kikuchi, M. Yamato and T. Okano, *Biomacromolecules*, 2012, **13**, 253–260.

64 M. Nakayama, T. Kanno, H. Takahashi, A. Kikuchi, M. Yamato and T. Okano, *Sci. Technol. Adv. Mater.*, 2021, **22**, 481–493.

65 K. Nagase, J. Kobayashi, A. Kikuchi, Y. Akiyama, H. Kanazawa and T. Okano, *Langmuir*, 2008, **24**, 511–517.

66 D. Xiao and M. J. Wirth, *Macromolecules*, 2002, **35**, 2919–2925.

67 M. Yamato, C. Konno, A. Kushida, M. Hirose, U. Mika, A. Kikuchi and T. Okano, *Biomaterials*, 2000, **21**, 981–986.

68 N. Asakawa, T. Shimizu, Y. Tsuda, S. Sekiya, T. Sasagawa, M. Yamato, F. Fukai and T. Okano, *Biomaterials*, 2010, **31**, 3903–3909.

69 M. Kanzaki, M. Yamato, J. Yang, H. Sekine, C. Kohno, R. Takagi, H. Hatakeyama, T. Isaka, T. Okano and T. Onuki, *Biomaterials*, 2007, **28**, 4294–4302.

70 A. Kushida, M. Yamato, C. Konno, A. Kikuchi, Y. Sakurai and T. Okano, *J. Biomed. Mater. Res.*, 2000, **51**, 216–223.

71 R. Suzuki, A. Aruga, H. Kobayashi, M. Yamato and M. Yamamoto, *Anticancer Res.*, 2014, **34**, 4747.

72 J. Akimoto, M. Nakayama, S. Takagi and T. Okano, *Anticancer Res.*, 2018, **38**, 671.

73 J. Akimoto, M. Nakayama, S. Takagi and T. Okano, *J. Biomed. Mater. Res., Part A*, 2019, **107**, 1071–1079.

74 Y. Iwase, M. Nakayama, M. Yamato and T. Okano, *Anticancer Res.*, 2015, **35**, 6481.

75 J. Lian, H. Xu, S. Duan, X. Ding, Y. Hu, N. Zhao, X. Ding and F.-J. Xu, *Biomacromolecules*, 2020, **21**, 732–742.

76 K. Nagase, A. Kimura, T. Shimizu, K. Matsuura, M. Yamato, N. Takeda and T. Okano, *J. Mater. Chem.*, 2012, **22**, 19514–19522.

77 K. Nagase, Y. Hatakeyama, T. Shimizu, K. Matsuura, M. Yamato, N. Takeda and T. Okano, *Biomacromolecules*, 2015, **16**, 532–540.

78 M. Husseman, E. E. Malmström, M. McNamara, M. Mate, D. Mecerreyes, D. G. Benoit, J. L. Hedrick, P. Mansky, E. Huang, T. P. Russell and C. J. Hawker, *Macromolecules*, 1999, **32**, 1424–1431.

79 M. Ejaz, S. Yamamoto, K. Ohno, Y. Tsujii and T. Fukuda, *Macromolecules*, 1998, **31**, 5934–5936.

80 C. Yoshikawa, A. Goto, Y. Tsujii, T. Fukuda, T. Kimura, K. Yamamoto and A. Kishida, *Macromolecules*, 2006, **39**, 2284–2290.

81 K. Nagase, J. Matsuda, A. Takeuchi and Y. Ikemoto, *Surf. Interfaces*, 2023, **40**, 103058.

82 K. Nagase, K. Yamaoka, R. Shimane, N. Kojima, N. L. Yamada, H. Seto and Y. Fujii, *Surf. Interfaces*, 2024, **54**, 105268.

83 A. J. Zollinger and M. L. Smith, *Matrix Biol.*, 2017, **60–61**, 27–37.

84 X. Ding and K.-L. Yang, *Anal. Chem.*, 2013, **85**, 10710–10716.

85 K. Nagase, H. Wakayama, J. Matsuda, N. Kojima and H. Kanazawa, *Mater. Today Bio*, 2023, **20**, 100627.

86 K. Nagase, M. Nagaoka, J. Matsuda and N. Kojima, *Mater. Des.*, 2024, **239**, 112824.

87 K. Nagase, J. Kobayashi, A. Kikuchi, Y. Akiyama, M. Annaka, H. Kanazawa and T. Okano, *Langmuir*, 2008, **24**, 10981–10987.

88 K. Nagase, Y. Hatakeyama, T. Shimizu, K. Matsuura, M. Yamato, N. Takeda and T. Okano, *Biomacromolecules*, 2013, **14**, 3423–3433.

89 K. Nagase, A. Ota, T. Hirotani, S. Yamada, A. M. Akimoto and H. Kanazawa, *Macromol. Rapid Commun.*, 2020, **41**, 2000308.

90 K. Nagase, M. Shimura, R. Shimane, K. Hanaya, S. Yamada, A. M. Akimoto, T. Sugai and H. Kanazawa, *Biomater. Sci.*, 2021, **9**, 663–674.

91 K. Nagase, N. Kojima, M. Goto, T. Akaike and H. Kanazawa, *J. Mater. Chem. B*, 2022, **10**, 8629–8641.

